early in DNA damage response and regulate RAP80 localization.

Many cell cycle checkpoint proteins, including ATM, Chk2, BRCA1, and p53, play critical roles in the maintenance of genomic stability. Their mutation often results in increased tumor incidence, highlighting the importance of the integrity of DNA damage pathways in tumor suppression. As a BRCA1-associated protein involved in DNA damage checkpoint control, RAP80 may also function as a tumor suppressor and be dysregulated or mutated in human patients. Future genetic studies will allow us to test this possibility.

References and Notes

1. B. B. Zhou, S. J. Elledge, *Nature* **408**, 433 (2000).
2. J. Rouse, S. P. Jackson, *Science* **297**, 547 (2002).
3. W. C. Hahn, R. A. Weinberg, *N. Engl. J. Med.* **347**, 1593 (2002).
4. T. T. Su, *Annu. Rev. Genet.* **40**, 187 (2006).
5. F. J. Couch *et al.*, *N. Engl. J. Med.* **336**, 1409 (1997).
6. D. Ford *et al.*, *Am. J. Hum. Genet.* **62**, 676 (1998).
7. R. Hashizume *et al.*, *J. Biol. Chem.* **276**, 14537 (2001).
8. A. Chen, F. E. Kleiman, J. L. Manley, T. Ouchi, Z. Q. Pan, *J. Biol. Chem.* **277**, 22085 (2002).
9. X. Yu, J. Chen, *Mol. Cell. Biol.* **24**, 9478 (2004).
10. S. B. Cantor *et al.*, *Cell* **105**, 149 (2001).
11. Z. Yan, Y. S. Kim, A. M. Jetten, *J. Biol. Chem.* **277**, 32379 (2002).
12. Materials and methods are available as supporting material on *Science* Online.
13. S. Hirano *et al.*, *Nat. Struct. Mol. Biol.* **13**, 272 (2006).
14. Single-letter abbreviations for the amino acid residues are as follows: A, Ala; C, Cys; D, Asp; E, Glu; F, Phe; G, Gly; H, His; I, Ile; K, Lys; L, Leu; M, Met; N, Asn; P, Pro; Q, Gln; R, Arg; S, Ser; T, Thr; V, Val; W, Trp; and Y, Tyr.
15. C. X. Deng, S. G. Brodie, *Bioessays* **22**, 728 (2000).
16. B. Xu, S. Kim, M. B. Kastan, *Mol. Cell. Biol.* **21**, 3445 (2001).
17. Q. Liu *et al.*, *Genes Dev.* **14**, 1448 (2000).
18. H. Takai *et al.*, *Genes Dev.* **14**, 1439 (2000).
19. R. I. Yarden, S. Pardo-Reoyo, M. Sgagias, K. H. Cowan, L. C. Brody, *Nat. Genet.* **30**, 285 (2002).
20. P. B. Deming *et al.*, *Proc. Natl. Acad. Sci. U.S.A.* **98**, 12044 (2001).
21. X. Yu, S. Fu, M. Lai, R. Baer, J. Chen, *Genes Dev.* **20**, 1721 (2006).
22. X. Wang, P. R. Andreassen, A. D. D'Andrea, *Mol. Cell. Biol.* **24**, 5850 (2004).
23. R. Montes de Oca *et al.*, *Blood* **105**, 1003 (2005).
24. We thank J. Wood for proofreading the manuscript; J. Hohfeld and B. Horazdovsky for providing constructs encoding HSJ1A and Ubi-GST, respectively; and A. D'Andrea for providing FANCD2-deficient and FANCD2-reconstituted cells. This work was supported by grants from NIH (grant number RO1CA089239 to J.C.), the Ovarian Cancer Research Fund (X.Y.), the University of Michigan Cancer Center Developmental Fund (X.Y.), the U.S. Department of Defense (DOD) Era of Hope Scholars Award (J.C.), and the DOD Breast Cancer Research Program Idea Award (X.Y.).

How Synaptotagmin Promotes Membrane Fusion

Sascha Martens,[1] Michael M. Kozlov,[2] Harvey T. McMahon[1]*

Synaptic vesicles loaded with neurotransmitters are exocytosed in a soluble *N*-ethylmaleimide–sensitive factor attachment protein receptor (SNARE)–dependent manner after presynaptic depolarization induces calcium ion (Ca^{2+}) influx. The Ca^{2+} sensor required for fast fusion is synaptotagmin-1. The activation energy of bilayer-bilayer fusion is very high ($\approx 40\ k_BT$). We found that, in response to Ca^{2+} binding, synaptotagmin-1 could promote SNARE-mediated fusion by lowering this activation barrier by inducing high positive curvature in target membranes on C2-domain membrane insertion. Thus, synaptotagmin-1 triggers the fusion of docked vesicles by local Ca^{2+}-dependent buckling of the plasma membrane together with the zippering of SNAREs. This mechanism may be widely used in membrane fusion.

At the synapse, neurotransmitter release is mediated by the Ca^{2+}-induced fusion of transmitter-loaded synaptic vesicles with the presynaptic plasma membrane. The plasma membrane–localized target (t)-SNAREs ([soluble *N*-ethylmaleimide–sensitive factor attachment protein 25 (SNAP-25) and syntaxin-1]) and the vesicle (v)–localized v-SNARE (synaptobrevin) and synaptotagmin-1 (syt1) are involved in the Ca^{2+}-triggered fusion of synaptic vesicles with the plasma membrane (*1*). The three SNAREs are believed to bring the two membranes destined for fusion into close apposition. Syt1 has been shown to be the Ca^{2+} sensor responsible for Ca^{2+}-triggered fusion (*2*), but the molecular mechanism by which syt1 accomplishes this is not fully understood. Syt1 is a vesicle-localized transmembrane protein with two cytoplasmic C2 domains, C2A and C2B (Fig. 1A). The C2A and the C2B domains each bind Ca^{2+}, which enables them to interact with membranes (*3, 4*). This activity is implicated in the triggering of membrane fusion (*5, 6*). In addition, Ca^{2+}-dependent and -independent interactions between syt1 with SNAREs have been shown (*7*).

The fusion of two membranes is now widely believed to occur through a hemifusion intermediate (*8*). For hemifusion to occur, high energy barriers must be overcome, which are thought to be related to the curvature deformations generated within the membranes during stalk formation and subsequent stages of membrane merging (*8, 9*). Syt1 has been shown to trigger Ca^{2+}-induced fusion and bind to membranes in a Ca^{2+}-dependent manner, and thus we investigated whether it could promote membrane fusion and, consequently, exocytosis, by affecting local membrane curvature.

Ca^{2+} binding by syt1 is mediated by a series of conserved aspartate residues that line pockets on one end of each of the C2A and C2B domains (*3, 10*) (Fig. 1A). We used a syt1 construct lacking the transmembrane domain but having the double C2 domain module (C2AB) (*11*). Ca^{2+} binding allows the C2A and C2B domains to interact with negatively charged phospholipids such as phosphatidylserine (PtdSer) and phosphatidylinositol-4,5-bisphosphate [PtdIns(4,5)P_2] (*12, 13*) (fig. S1). This interaction results in the insertion of four loops (two from each of the C2 domains) into the lipid bilayer (*14, 15*). M173, F234, V304, and I367 (*16*) located on the tips of the membrane-binding loops (Fig. 1A) penetrate to a third of the lipid monolayer depth (*15*). This kind of hydrophobic-loop insertion should generate a tendency for the monolayer to bend to relieve the tension created by the insertion. If syt1 contributes to spontaneous membrane curvature (*8*), the closer the membrane curvature is to that preferentially produced by syt1, the stronger the syt1 affinity for membrane binding should be. Conversely, addition of syt1 to initially flat membranes should induce a positive curvature.

We incubated liposomes of different sizes, and, consequently, of different curvatures, with syt1 C2AB domains in the presence and absence of 1 mM Ca^{2+}. The binding of syt1 to membranes was monitored by a cosedimentation assay (Fig. 1B). Syt1 showed a clear preference for binding smaller liposomes (Fig. 1, Bii and C). This effect was observed only in the presence of Ca^{2+}, whereas the Ca^{2+}-independent interaction of syt1 with liposomes was size independent (Fig. 1Bi). This positive-curvature preference was largely lost when we increased the strength of interaction of syt1 with the membrane by elevating the PtdSer content in the liposomes from 15 to 25% (Fig. 1D). Likewise, the binding to Folch liposomes, which are rich in PtdSer, was largely curvature independent. The syt1 C2AB domain

[1]Medical Research Council–Laboratory of Molecular Biology, Hills Road, CB2 0QH Cambridge, UK. [2]Department of Physiology and Pharmacology, Sackler Faculty of Medicine, Tel Aviv University, 69978 Tel Aviv, Israel.

*To whom correspondence should be addressed. E-mail: hmm@mrc-lmb.cam.ac.uk

thus lost its ability to sense membrane curvature when the strength of interaction with the membrane was increased. To determine if the insertion of the hydrophobic loops accounted for syt1's preferential binding to small liposomes, we mutated M173, F234, V304, and I367 to alanines (4A mutant). The 4A mutant bound to 0.8-μm liposomes with an affinity similar to that of wild-type syt1 but showed no increased binding to small liposomes (Fig. 1, Biii and C). A mutant with all four residues mutated to tryptophans (4W mutant) showed an increased curvature preference (Fig. 1, Biv and C), but like the wild-type C2AB domain, lost its curvature preference when the PtdSer content in the liposomes was increased to 25%. Another mutant, K326E, with a point mutation in the polybasic region of the C2B domain that is remote from the Ca^{2+}-dependent membrane interaction site (Fig. 1A), was defective in Ca^{2+}-independent binding to liposomes but showed unaltered Ca^{2+}-mediated membrane interactions (fig. S1). Furthermore, as expected, K326E bound more effectively to small liposomes (Fig. 1, Bv and C).

To determine if syt1 could induce positive membrane curvature, we incubated Folch liposomes with syt1 in the presence and absence of Ca^{2+}. We observed extensive tubulation of Folch liposomes by syt1 only in the presence of Ca^{2+} (Fig. 2, A and B). The average diameter of tubules was 17.5 ± 3 nm from outer bilayer to outer bilayer, showing that the interaction of syt1 with membranes results in the induction of high positive curvature. For comparison, the N-BAR module (Bin/amphiphysin/Rvs domain with an N-terminal amphipathic helix) of amphiphysin makes lipid tubules of 46 nm (17). Using the syt1 C2A and C2B crystal structures (3, 10) and the depth of insertions determined by electron paramagnetic resonance spectroscopy (15), we estimated that ~30% of the tubular surface needs to be covered to stabilize this curvature.

The tubulation of liposomes required the C2A and C2B domains to be linked to each other; the separated C2A and C2B domains did not tubulate Folch liposomes in the presence of Ca^{2+} (Fig. 2C). The 4A mutant failed to induce tubulation of Folch liposomes; in contrast, the 4W mutant caused tubulation and fragmentation of the liposomes, indicating further destabilization of the membrane (Fig. 2, D and E, and fig. S2). This destabilization is likely to have resulted from the greater volume occupied by the bulkier residues within the monolayer. The K326E mutant showed tubulation to an extent similar to that shown by the wild-type C2AB fragment (Fig. 2F). A C2AB fragment with mutations in the Ca^{2+}-binding site of the C2A domain (D230N, D232N) tubulated Folch liposomes (Fig. 2G), whereas a C2AB fragment with mutations in the Ca^{2+}-binding site of the C2B domain (D363N, D365N) did not induce membrane curvature (Fig. 2H). These

results correlate with the ability of the former and inability of the latter mutant to promote synaptic vesicle exocytosis in vivo (18, 19). We next investigated whether the tubulation of liposomes required the specific presence of the C2A and the C2B domains by fusing two C2A domains (C2AA) and two C2B domains (C2BB) and incubating them with liposomes in the presence of Ca^{2+}. Both fragments tubulated liposomes (Fig. 2, I and J), suggesting that the requirement for the induction of positive membrane curvature is the presence of two tethered C2 domains and their penetration of the lipid monolayer.

Next, we examined whether the Ca^{2+}-dependent induction of membrane curvature by syt1 is required for the promotion of SNARE-mediated membrane fusion in an in vitro assay (11, 20, 21). SNAREs alone were inefficient in promoting fusion of liposomes (Fig. 3A). Full-length syt1 had no effect in this assay but, as expected (21), we observed accelerated fusion by the addition of syt1 C2AB domain only in the presence of Ca^{2+} (Fig. 3A). This effect depended absolutely on the presence of SNAP-25 and syntaxin-1 in the target liposomes (Fig. 3A). The C2A and C2B domains had to be linked in order to promote membrane fusion (fig. S3) (21). The 4A mutant was unable to promote membrane fusion, whereas the 4W mutant showed increased

promotion of membrane fusion compared with the wild-type C2AB fragment (Fig. 3B). Indeed, the expression in hippocampal neurons of a mutant syt1 carrying tryptophans in the membrane-binding loops results in an increased probability of synaptic vesicle release (6). The inability of the 4A mutant to promote membrane fusion was not due to its lower affinity for membranes, because increasing the concentration of the 4A mutant in the membrane fusion assay did not lead to increased fusion but rather led to a slight inhibition, perhaps due to masking of phospholipids (fig. S3). The K326E mutant, which could induce membrane curvature (Fig. 2), promoted membrane fusion to an extent similar to that shown by the wild-type protein, suggesting that the polybasic stretch was not required for the promotion of fusion in vitro (Fig. 3B). These results correlate well with the ability of wild-type syt1 and the syt1 mutants to induce tubulation of liposomes (Fig. 2).

Next, we tested the syt1 C2AA and C2BB domains for their ability to promote SNARE-dependent membrane fusion (Fig. 3C). Both proteins were indeed able to tubulate liposomes (Fig. 2). In our fusion assay, however, the C2AA domain was unable to promote fusion, whereas the C2BB domain was even more active than the syt1 C2AB domain, indicating that the induction
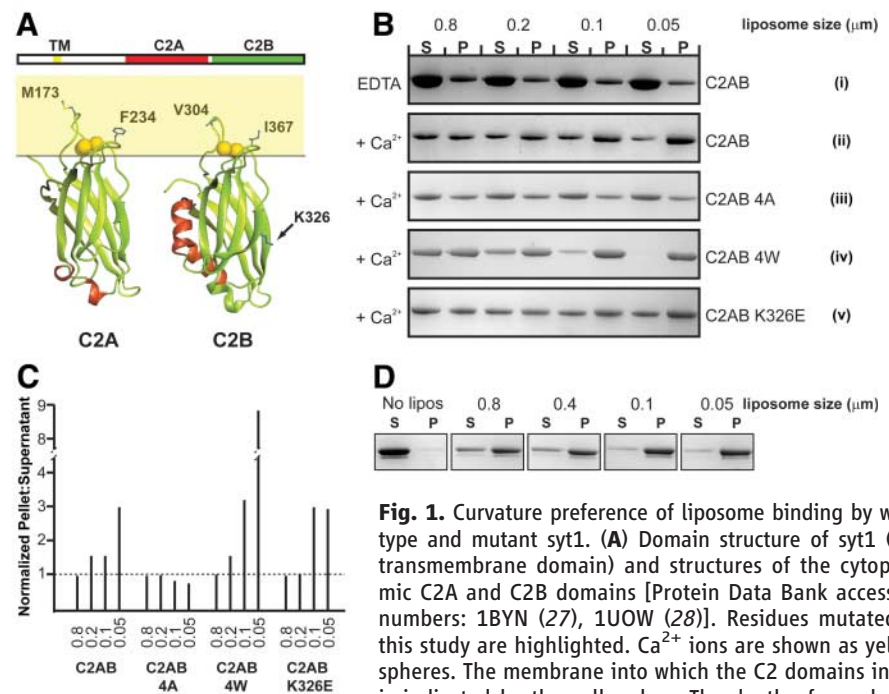

Fig. 1. Curvature preference of liposome binding by wild-type and mutant syt1. (**A**) Domain structure of syt1 (TM: transmembrane domain) and structures of the cytoplasmic C2A and C2B domains [Protein Data Bank accession numbers: 1BYN (27), 1UOW (28)]. Residues mutated in this study are highlighted. Ca^{2+} ions are shown as yellow spheres. The membrane into which the C2 domains insert is indicated by the yellow box. The depth of membrane insertion is shown according to (15). (**B**) Lipid cosedimentation assay. The indicated proteins were incubated with liposomes of different sizes (0.8 to 0.05 μm) in the absence (1 mM EDTA) or presence of 1 mM Ca^{2+}. P, pellet formed by centrifuging; S, supernatant. Representative gels from one of three independent experiments are shown. (**C**) Quantification of lipid cosedimentation experiments presented in (B). The P/S ratio for the 0.8-μm liposomes was set to 1. The numbers indicate the size of the liposomes (in micrometers). (**D**) The curvature preference of syt1 for smaller liposomes is largely lost when the PtdSer content is increased to 25%, as determined by liposome cosedimentation. The numbers indicate the size of the liposomes used for cosedimentation.

of membrane curvature alone is not sufficient to promote fusion. We attribute the lack of fusion-promoting activity by the C2AA domain to its inability to correctly interact with the SNARE complex, whereas the C2BB domain might be better positioned in respect to the SNARE complex. The C2B domain interacts more strongly with the SNARE complex (*22*).

We further tested the syt4 C2AB domain in our fusion assay. Syt4 lacks Ca^{2+}-dependent phospholipid-binding activity and did not tubulate Folch liposomes (fig. S1), but it displays SNARE binding to an extent similar to that shown by the syt1 C2AB domain (*23*). The syt4 C2AB domain failed to promote fusion (Fig. 3C), indicating that membrane binding and defor-

mation by synaptotagmins are essential for the promotion of membrane fusion.

We further tested three synaptotagmin-related proteins—syt3, syt9, and synaptotagmin-like protein 2 (slp2)—for the induction of membrane curvature (Fig. 3). Syt3 and syt9 showed substantial Ca^{2+}-independent binding to liposomes, which increased upon the addition of Ca^{2+}, whereas the binding of slp2 to Folch liposomes was not affected by Ca^{2+} (Fig. 3D). Syt3 and syt9 both tubulated Folch liposomes in a Ca^{2+}-dependent manner, whereas slp2 tubulation did not require Ca^{2+} (Fig. 3E). The induction of positive curvature in the target membrane thus appears to be a property shared by many double C2 domain–containing proteins.

We propose the following model for the action of syt1 during Ca^{2+}-dependent synaptic vesicle release (fig. S4). Because of its Ca^{2+}-independent interaction with the tSNAREs and/or PtdIns(4,5)P$_2$ in the plasma membrane (*13, 24*), syt1 in the synaptic vesicle is closely associated with the trans-SNARE complexes, which have been suggested to be ordered ringwise around the future fusion site (*20*). Upon Ca^{2+} influx and subsequent Ca^{2+} binding by syt1, the C2A and C2B domains penetrate the plasma membrane, resulting in the local induction of positive membrane curvature under the SNARE complex ring. This causes buckling toward the synaptic vesicle of the plasma membrane within the SNARE ring, reducing the distance between the two membranes. Furthermore, the buckled membrane is under curvature stress, which reduces the energy barrier the membrane has to overcome at the intermediate stage of fusion and, hence, accelerates the fusion reaction. An estimate of the energy released on going from buckle to stalk formation is 20 $k_B T$. This reduces the overall energy of stalk formation from ~40 $k_B T$ (*9*) to about 20 $k_B T$ (*11*). The remaining energy can be overcome by the membrane spontaneously (*9, 25*). According to our model, syt1 has to bind the SNARE complex in order to target the membrane buckle under the vesicle. Indeed, the failure of syt1 to promote yeast SNARE-mediated membrane fusion correlates with its inability to bind the yeast SNAREs (*26*).

We have shown that, for syt1, the multiple C2 domain (MC2D) module promotes membrane fusion by the Ca^{2+}-dependent induction of membrane curvature, explaining how syt1 couples Ca^{2+} entry into a synapse to vesicle fusion. MC2D-containing proteins are found throughout the eukaryotic kingdom and constitute a large protein superfamily that includes molecules such as synaptotagmin-like proteins, ferlins, rabphilin, Rim, and DOC2. The promotion of membrane fusion by local induction of membrane curvature stress by MC2D-containing proteins may thus be a widespread phenomenon.
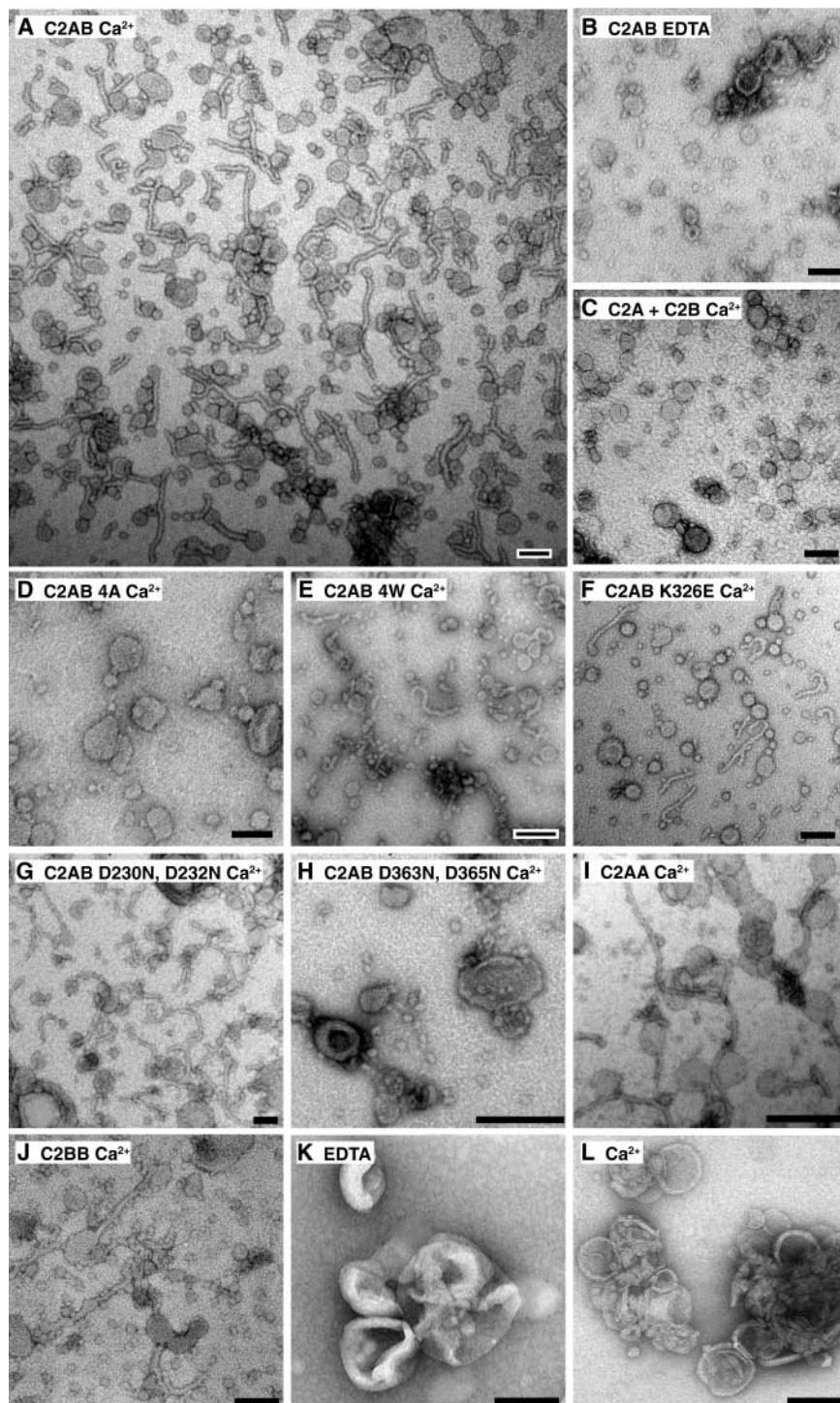

Fig. 2. Ca^{2+}-dependent induction of positive membrane curvature seen as tubulation by wild-type and mutant syt1. (**A** to **L**) Electron micrographs of Folch liposomes incubated with the indicated proteins at a concentration of 10 μM (*11*). Scale bar: 100 nm.

References and Notes
1. T. C. Sudhof, *Annu. Rev. Neurosci.* **27**, 509 (2004).
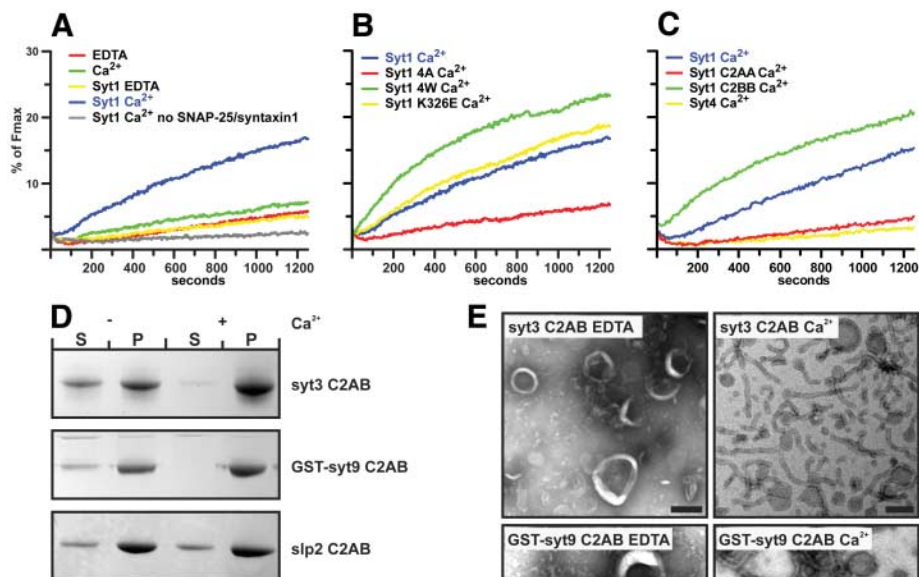2. M. Geppert *et al.*, *Cell* **79**, 717 (1994).

Fig. 3. Reconstitution of membrane fusion in vitro and liposome-binding and tubulation by synaptotagmin-related proteins. (**A**) Fusion of tSNARE and vSNARE liposomes was monitored by dequenching of NBD [*N*-(7-nitro-2-1, 3-benzoxadiazol-4-yl] upon lipid mixing. Syt1 was added at a concentration of 7.5 μM and Ca^{2+} was added to a final concentration of 500 μM. The maximal fluorescence (F$_{max}$) was determined by the addition of 1% Triton X-100. (**B**) Same fusion assay as in (A), showing the indicated syt1 mutants used at a concentration of 7.5 μM. (**C**) Fusion assay as in (A) with the C2AB, C2AA, C2BB, and syt4 C2AB domains at a concentration of 7.5 μM. (**D**) Co-sedimentation assay using Folch liposomes and the indicated proteins. (**E**) Electron micrographs of Folch liposomes incubated with the indicated proteins. Ca^{2+} was added to a final concentration of 1 mM in (D) and (E). Scale bar: 100 nm.

3. I. Fernandez *et al.*, *Neuron* **32**, 1057 (2001).
4. B. A. Davletov, T. C. Sudhof, *J. Biol. Chem.* **268**, 26386 (1993).
5. R. Fernandez-Chacon *et al.*, *Nature* **410**, 41 (2001).
6. J. S. Rhee *et al.*, *Proc. Natl. Acad. Sci. U.S.A.* **102**, 18664 (2005).
7. J. Tang *et al.*, *Cell* **126**, 1175 (2006).
8. L. V. Chernomordik, M. M. Kozlov, *Annu. Rev. Biochem.* **72**, 175 (2003).
9. Y. Kozlovsky, M. M. Kozlov, *Biophys. J.* **82**, 882 (2002).
10. R. B. Sutton, B. A. Davletov, A. M. Berghuis, T. C. Sudhof, S. R. Sprang, *Cell* **80**, 929 (1995).
11. Materials and methods and calculations are available as supporting material on *Science* Online.
12. M. S. Perin, V. A. Fried, G. A. Mignery, R. Jahn, T. C. Sudhof, *Nature* **345**, 260 (1990).
13. J. Bai, W. C. Tucker, E. R. Chapman, *Nat. Struct. Mol. Biol.* **11**, 36 (2004).
14. E. Hui, J. Bai, E. R. Chapman, *Biophys. J.* **91**, 1767 (2006).
15. D. Z. Herrick, S. Sterbling, K. A. Rasch, A. Hinderliter, D. S. Cafiso, *Biochemistry* **45**, 9668 (2006).
16. Single-letter abbreviations for the amino acid residues used are as follows: A, Ala; D, Asp; F, Phe; K, Lys; L, Leu; M, Met; V, Val; and W, Trp.
17. B. J. Peter *et al.*, *Science* **303**, 495 (2004).
18. I. M. Robinson, R. Ranjan, T. L. Schwarz, *Nature* **418**, 336 (2002).
19. J. M. Mackler, J. A. Drummond, C. A. Loewen, I. M. Robinson, N. E. Reist, *Nature* **418**, 340 (2002).
20. T. Weber *et al.*, *Cell* **92**, 759 (1998).
21. W. C. Tucker, T. Weber, E. R. Chapman, *Science* **304**, 435 (2004).
22. H. Dai, N. Shen, D. Arac, J. Rizo, *J. Mol. Biol.* **367**, 848 (2007).
23. C. Rickman, M. Craxton, S. Osborne, B. Davletov, *Biochem. J.* **378**, 681 (2004).
24. C. Rickman *et al.*, *Mol. Biol. Cell* **17**, 283 (2006).
25. P. I. Kuzmin, J. Zimmerberg, Y. A. Chizmadzhev, F. S. Cohen, *Proc. Natl. Acad. Sci. U.S.A.* **98**, 7235 (2001).
26. A. Bhalla, M. C. Chicka, W. C. Tucker, E. R. Chapman, *Nat. Struct. Mol. Biol.* **13**, 323 (2006).
27. X. Shao, I. Fernandez, T. C. Sudhof, J. Rizo, *Biochemistry* **37**, 16106 (1998).
28. Y. Cheng *et al.*, *Protein Sci.* **13**, 2665 (2004).
29. We thank B. Davletov for the provision of synaptotagmin 3, 4, and 9 plasmids and members of the lab for extensive discussions. This work was supported by the Medical Research Council (UK). We also gratefully acknowledge a long-term fellowship from the European Molecular Biology Organization (ALTF 21-2006) to S.M. and the Israel Science Foundation, United States–Israel Binational Science Foundation, and the Marie Curie Network "Flippases" funding for M.M.K.

Myosin V Walks by Lever Action and Brownian Motion

Katsuyuki Shiroguchi and Kazuhiko Kinosita Jr.*

Myosin V is a molecular motor that moves cargo along actin filaments. Its two heads, each attached to a long and relatively stiff neck, move alternately forward in a "hand-over-hand" fashion. To observe under a microscope how the necks move, we attached a micrometer-sized rod to one of the necks. The leading neck swings unidirectionally forward, whereas the trailing neck, once lifted, undergoes extensive Brownian rotation in all directions before landing on a site ahead of the leading head. The neck-neck joint is essentially free, and the neck motion supports a mechanism where the active swing of the leading neck biases the random motion of the lifted head to let it eventually land on a forward site.

Linear molecular motors such as myosin, kinesin, or dynein are often Y-shaped, with two identical arms of Y each ending in a globular motor domain that binds to a track in an adenosine triphosphate (ATP)–dependent manner. Traditionally the motor domain has been called a "head" and the rest of the arm a "neck" (Fig. 1A). How the heads and necks cooperate to propel the motor is best understood in those motors that take many discrete steps without falling off a filamentous track (*1–7*): The two heads move forward alternately in a "hand-over-hand" fashion, as in human walking (*8–11*). However, the mechanism for bringing the lagging head onto a forward landing site is not yet firmly established. Here we focus on myosin V (*12*, *13*) that walks on an actin filament with ~35-nm steps (*14*, *15*). The necks of this motor are stiff relative to those of other motors such as kinesin, and they are called "lever arms" because they would serve as a lever. In electron micrographs (*16*), myosin V's long necks form a V-shape when both heads are attached to actin. Every step would thus result in leaning of a neck alternately forward and backward, as indeed was shown when a fluorophore

Department of Physics, Faculty of Science and Engineering, Waseda University, Okubo 3-4-1, Shinjuku-ku, Tokyo 169-8555, Japan.

*To whom correspondence should be addressed. E-mail: kazuhiko@waseda.jp

Supporting Online Material for

How Synaptotagmin Promotes Membrane Fusion

Sascha Martens, Michael M. Kozlov, Harvey T. McMahon[*]

*To whom correspondence should be addressed. E-mail: hmm@mrc-lmb.cam.ac.uk

This PDF file includes:

> Materials and Methods
> SOM Text
> Figs. S1 to S6
> References

Correction: In the "Protein expression" section of the Materials and Methods, it was incorrectly stated that the C2B domain construct of synaptotagmin ended in residue 408. It should have read: "The C2B domain comprised amino acids 273–421."

Supporting Online Material for

How Synaptotagmin Promotes Membrane Fusion

Sascha Martens[1], Michael M. Kozlov[2] and Harvey T. McMahon[1*]

[1] MRC-Laboratory of Molecular Biology, Hills Road, CB2 0QH Cambridge, UK

[2] Department of Physiology and Pharmacology, Sackler Faculty of Medicine, Tel Aviv University, 69978 Tel Aviv, Israel

*To whom correspondence should be addressed. E-mail: hmm@mrc-lmb.cam.ac.uk

This PDF file includes:

Material and Methods

Protein expression

All synaptotagmin fragments were expressed as GST fusion proteins from pGEX4T2 or pGEX4T1. The C2AB domain constructs comprised amino acids 96-421 of rat synaptotagmin-1. The C2A domain comprised amino acids 142-262 of rat synaptotagmin-1 and the C2B domain comprised amino acids 273-421. Mutations into the C2AB domain construct were introduced according to the Stratagene Quick Change protocol (see Fig. S5 for a list of mutants). The syt3, syt4 and syt9 C2AB domain fragments are described in *(S1)*. The slp2 C2AB domain fragment comprised amino acids 597-910 of human slp2a.

The C2AA domain construct was generated as follows: A fragment containing the cytoplasmic linker (starting at amino acid 96) connecting the transmembrane with the C2A domain, the C2A domain and the linker between the C2A and C2B domain was amplified by PCR and cloned into pGEX4T1 via BamHI-SalI. Subsequently a PCR-fragment containing only the C2A domain was cloned into the construct containing the first fragment via SalI-NotI.

The C2BB domain construct was generated as follows: First a fragment comprising the cytoplasmic linker (starting at amino acid 96) connecting the transmembrane with the C2A domain was amplified by PCR and cloned into pGEX-4T1 via BamHI-EcoRI. Then a fragment comprising the C2B domain was cloned into the vector containing the cytoplasmic linker via EcoRI-SalI. Finally a fragment containing the linker between the C2A and C2B domain and the C2B domain was cloned into the vector containing the first two fragments via SalI-NotI.

For expression of the syt1 C2AB, C2A, C2B, C2AA and C2BB domain fragments and the syt3 C2AB, syt4 C2AB and slp2 C2AB domain fragments BL21(DE3) pLysS cells (Stratagene) were used. Cells were grown at 37°C until OD_{600} of 0.3, induced with 40μM IPTG and grown for 14-16h at 18°C. Cells were harvested and resuspended in 50mM HEPES pH7.5, 300mM NaCl, 4mM DTT, 2mM $MgCl_2$, DNaseI, RNaseA and lysed by freeze thawing. The lysate was centrifuged for 45 min at 125,000g, 4°C and the supernatant was incubated with 1ml of glutathione beads (GE healthcare) per 1l of culture for 1-2h. Beads were washed 7 times with 50mM HEPES pH 7.5, 300mM NaCl, 4mM DTT followed by two 15min washes with 50mM HEPES pH7.5, 500mM NaCl, 2mM $MgCl_2$, DNaseI, RNaseA. The protein was cleaved off the beads with thrombin by over night incubation at 4°C. The supernatant was concentrated and the protein was further purified by gelfiltration in 50mM HEPES pH7.5, 150mM NaCl, 4mM DTT using a HiLoad 16/60 Superdex 75 column (Pharamcia Biotech). For the 4W mutant the gelfiltration was conducted with 300mM NaCl instead of 150mM NaCl. The syt9 C2AB domain fragment was purified as described above except that the protein was eluted from the glutathione beads with 100mM glutathione and subsequently gelfiltered. GST-syt9 C2AB was used for the experiments. The proteins were shock frozen and stored at -80°C. Possible protein and RNA contamination was checked by SDS gel electrophoresis and UV spectroscopy, respectively.

Rat full length SNAP-25 and full length synatxin1 were expressed as GST fusion proteins in BL21(DE3) pLysS cells (Stratagene). Cells were grown at 37°C until OD600 of 0.9-1, induced with 500μM IPTG and grown for 4h at 37°C. Cells were harvested and resuspended in 50mM Tris pH8, 300mM KCl, 10% glycerol, 5% Triton X-100, 5mM DTT, 2mM $MgCl_2$, DNaseI, EDTA-free Complete protease inhibitors (Roche) and lysed by freeze thawing. The lysate was centrifuged for 45 min at

125,000g, 4°C and the supernatant was incubated with 1ml of glutathione beads (GE Healthcare) per 1l of culture for 1-2h. Beads were washed 6x with 50mM Tris pH8, 300mM KCl, 10% glycerol, 1% Triton X-100, 5mM DTT, EDTA-free Complete protease inhibitors (Roche) and subsequently washed with over 20 bead volumes of 50mM Tris pH8, 100mM KCl, 0.8% w/v n-octyl β-D-glucopyranoside (OGP), 5mM DTT. SNAP-25 and syntaxin-1a were cleaved off the beads with thrombin over night at 4°C. Thrombin was then inactivated by the addition of 0.1mM PMSF followed by 1h incubation at room temperature. The supernatant was shock frozen and stored at -80°C.

Rat full length synaptobrevin was expressed as GST fusion protein from pGEX4T1 in BL21(DE3) pLysS cells. Cells were grown at 37°C until OD_{600} of 0.3, induced with 40μM IPTG and grown for 14-16h at 18°C. Cells were harvested and resuspended in 25mM HEPES pH7.5, 400mM KCl, 5% Triton X-100, 10% glycerol, 2mM MgCl$_2$, 4mM DTT, EDTA-free Complete protease inhibitors (Roche), 0.2mM PMSF, DNaseI. Cells were lysed by freeze thawing and the lysate was centrifuged for 45 min at 125,000g, 4°C and the supernatant was incubated with 1ml of glutathione beads (GE healthcare) per 1l of culture for 1-2h. Beads were washed 6x with 25mM HEPES pH7.5, 400mM KCl, 5% Triton X-100, 10% glycerol, 4mM DTT, EDTA-free Complete protease inhibitors (Roche) and subsequently with 25mM HEPES pH7.5, 100mM KCl, 10% glycerol, 1% w/v OGP, 4mM DTT. Synaptobrevin was cleaved off the beads with thrombin over night at 4°C. Thrombin was then inactivated by the addition of 0.1mM PMSF followed by 1h incubation at room temperature. The supernatant was shock frozen and stored at -80°C.

The functionality of SNAP25, syntaxin1 and synaptobrevin was monitored by SDS-resistant SNARE complex formation (S2) which is show in (Fig. S6).

Reconstitution of membrane fusion

The tSNARE and vSNARE liposomes were prepared by detergent assisted insertion into preformed liposomes.

tSNARE liposomes: To create a 20mM liposome suspension lipids stored in chloroform were mixed in the following ratio: 25% phosphatidylserine (PtdSer) (Avanti #840032), 10% cholesterol (Sigma), 65% phosphatidylcholine (PtdChol) (Avanti #840053). For the experiment shown in Fig. S3 5% phosphatidyinosotol-4,5-bisphosphate (PtdIns(4,5)P$_2$) (Avanti #840046) was used and the amount of PtdChol was correspondingly decreased. Lipids were dried under argon and desiccated for 2h. Lipids were rehydrated by the addition of 50mM Tris pH8, 150mM NaCl, 2mM DTT. Lipids were incubated in the buffer for 15 min at room temperature and subsequently sonicated gently. The liposomes were then passed 9 times though an 800 nm filter (Whatman). 10μl of the liposomes were then added to 90μl of a 11.1μM tSNARE complex solution and incubated for 15 min at room temperature. The detergent was then diluted below the critical micelle concentration by the addition of 100μl 50mM Tris pH8, 150mM NaCl, 2mM DTT. The liposomes were then dialyzed over night against 2l of 25mM HEPES pH7.5, 100mM KCl, 5% glycerol, 2mM DTT, 10g BioBeads (BioRad) at 4°C to remove the detergent and spun at 10,000g for 5 min at room temperature to remove aggregates. The supernatant was used for experiments.

vSNARE liposomes: To create a 10mM liposome suspension lipids stored in chloroform were mixed in the following ratio: 15% phosphatidylserine (PtdSer) (Avanti #840032), 10% cholesterol (Sigma), 72% phosphatidylcholine (PtdChol) (Avanti #840053), 1.5% N-(7-nitro-2-1,3-benzoxadiazol-4-yl)-1,2-dipalmitoyl phosphatidylethanolamine (Invitrogen) and 1.5% rhodamine-

phosphatidylethanolamine (Invitrogen), dried under argon and desiccated for 2h. Lipids were rehydrated by the addition of 50mM Tris pH8, 150mM NaCl, 2mM DTT. Lipids were incubated in the buffer for 15 min at room temperature and sonicated gently. The liposomes were then passed 21 times though a 400 nm filter (Whatman) and subsequently through a 50 nm filter (Whatman). $20\mu l$ of the liposomes were the added to $80\mu l$ of a $50\mu M$ solution of synaptobrevin and incubated for 15 min at room temperature. The detergent was then diluted below the critical micelle concentration by the addition of $100\mu l$ 50mM Tris pH8, 150mM NaCl, 2mM DTT. The liposomes were then dialyzed over night against 2l of 25mM HEPES pH7.5, 100mM KCl, 5% glycerol, 2mM DTT, 10g BioBeads (BioRad) over night at $4^{\circ}C$ to remove the detergent and spun at 10,000g for 5 min at room temperature to remove aggregates. The supernatant was used for experiments.

The size of the reconstituted t- and vSNARE liposomes was checked by dynamic light scattering. The t- and vSNARE liposomes had an average hydrodynamic radius of 60-70nm and polydispersity index of 0.14-0.17.

The integrity of both the tSNARE and vSNARE liposomes was checked by negative stain electron microscopy and incubation with Botulinum neurotoxin E or Tetanus toxin. As expected for random integration into liposomes only 50% of SNAP-25 and synaptobrevin, respectively were cleaved. As analyzed by electron microscopy the tSNARE liposomes contained a significant number of larger liposomes (>200nm) as compared to the vSNARE lipsosomes.

For the fusion experiments $75\mu l$ tSNARE liposomes were mixed with $25\mu l$ vSNARE liposomes. The syt1 C2A, C2B, C2AB, C2AA, C2BB and syt4 C2AB domains were added at a concentration of $7.5\mu M$. The reactions were incubated on ice for 30 min before measurement. Ca^{2+} was added immediately before the measurement to final concentration of $500\mu M$. Fusion was monitored by dequenching of NBD. The NBD was excited at 465nm and emission was detected at 530nm. After 50 min 10% Triton X-100 was added to a final concentration of 1% to determine the maximum fluorescence. Synaptotagmin has been shown to promote full fusion of tSNARE and vSNARE liposomes under these conditions (S3). A slight condensation occurs on the outside of the cuvette on moving to 37°C (t=0) the temperature at which measurements are made. This precludes an accurate measurement of the initial rates.

Co-sedimentation assays

Liposomes were prepared using either Folch lipids (fraction1, Sigma), 5% PtdIns(4,5)P$_2$ (Avanti #840046), 10% cholesterol (Sigma), 15% PtdSer (Avanti #840032), 70% PtdChol (Avanti #840053) (Fig. 2A and Fig. S1B), 5% PtdIns(4,5)P$_2$ (Avanti #840046), 10% cholesterol (Sigma), 25% PtdSer (Avanti #840032), 60% PtdChol (Avanti #840053) (Fig. 2C) or varying amounts of PtdSer, PtdChol and 10% cholesterol as indicated in Fig. S1A. Lipids were combined, dried under argon, desiccated for 2h and buffer was added to a final concentration of 1mg/ml liposomes. 0.5mg/ml liposomes were incubated with $20\mu g$ of the proteins indicated in the figures. Ca^{2+} and EDTA were added to a final concentration of 1mM. After 30 min at room temperature the liposomes were centrifuged at 165,000g for 10 min at room temperature. Equal amounts of the supernatants and pellets were loaded. Proteins were subsequently visualized by Coomassie staining after SDS-PAGE. The liposomes shown in Fig. 2A and Fig. 2C were sequentially passed 9x though an 800nm filter, 21x through a 200nm filter, 21x times through a 100nm filter and 21x trough a 50 nm filter. The average hydrodynamic diameter of the liposomes shown in Fig. 1B as determined by dynamic light scattering was 290nm (Pdl 0.266) for the 800nm

liposomes, 124nm (Pdl 0.139) for the 200nm liposomes, 104nm for the 100nm (Pdl 0.086) liposomes and 71.9nm (Pdl 0.068) for the 50nm liposomes. The average hydrodynamic diameter of the liposomes shown in Fig. 1D as determined by dynamic light scattering was 291nm (Pdl 0.308) for the 800nm liposomes, 156nm (Pdl 0.087) for the 200nm liposomes, 118nm (Pdl 0.083) for the 100nm liposomes and 74nm (Pdl 0.042) for the 50 nm liposomes. Pdl indicates the polydispersity index. The actual size of the liposomes is significantly smaller for the 800 and 200 liposomes suggesting that the actual curvature preference of the synaptotagmin C2AB domain shown in Fig. 1B is underestimated. The very similar size of the liposomes shown in Fig. 1B and Fig. 1D shows that the loss of curvature preference for the liposomes shown in Fig. 1D is not attributable to a smaller size of liposomes shown in Fig. 1D.

Liposome tubulation assay by negative stain electron microscopy
Folch lipids (fraction 1, Sigma) were dried under argon, desiccated for 2h and buffer was added to a final concentration of 1mg/ml liposomes. 0.3mg/ml Folch were incubated with 10μM syt1 C2A, C2B or C2AB domain fragments, 10μM syt3 C2AB, 10μM syt9 GST-C2AB or 15μM slp2 C2AB in the presence of 1mM EDTA or CaCl$_2$ for 1h at room temperature and stained with 2% uranylacetate. Folch liposomes were used because artificial liposomes as used previously (S*4*) tended to show deformations even in the absence of protein.

Calculations

Calculation of the synaptotagmin spontaneous curvature

To estimate the synaptotagmin spontaneous curvature J_s^{syt} we consider the elastic stresses and strains produced within a fragment of lipid monolayer by insertion of the hydrophobic segments of C2, and seek for the monolayer shape compensating the effects of these stresses.

We consider an initially flat monolayer fragment of area A_0 and thickness L. An inclusion characterized by an in-plane area ΔA is embedded into the monolayer fragment up to the depth d. As a result of this embedding, the upper part of the monolayer penetrated by the inclusion tends to expand its area up to $A_0 + \Delta A$, whereas the lower part tends to conserve its initial area A_0. The created area mismatch between the upper and lower portions of the monolayer fragment and the related elastic energy can be partially compensated by the monolayer bending, which will be characterized by the curvature J of the monolayer bottom surface. We will find the spontaneous curvature J_s by looking for the value of J corresponding to the minimal elastic energy of the monolayer fragment.

To describe the position along the monolayer thickness we use the coordinate along the axis z perpendicular to the monolayer plane and initiating at the monolayer bottom. We consider the monolayer fragment as consisting of infinitesimally thin sub-layers of thickness dz, each characterized by the area stretching-compression modulus $\lambda(z)$. The elastic energy of each sub-layer is given by

$$dF = \frac{1}{2} \cdot \lambda(z) \cdot \left[A(z) - A_S(z)\right]^2 dz \qquad (A1)$$

where $A(z)$ is actual area of the sub-layer, and $A_S(z)$ is the sub-layer spontaneous area corresponding to its unstressed state. The actual area $A(z)$ can be expressed through the area A and the total curvature J (S5) of the bottom monolayer plane by

$$A(z) = A \cdot \left(1 + z \cdot J\right) \qquad (A2)$$

(the Eq.(A2) relates to cylindrical shape and, therefore, neglects the effects of the Gaussian curvature (S5)).

We assume that the rigidity $\lambda(z)$ has the same value λ_0 everywhere except for a narrow region around the plane $z^* \approx \frac{2}{3}L$ of the lipid glycerol backbones, where the rigidity has a considerably higher value. This assumption takes into account that the so called neutral (S6) (or pivotal (S7)) plane of lipid monolayers is always localized close to the plane of the glycerol backbones., To express this assumption mathematically, we present the rigidity by $\lambda(z) = \lambda_0 + \Lambda \cdot \delta(z - z^*)$, where $\delta(z - z^*)$ is the delta-function.

According to our model, the spontaneous area $A_S(z)$ equals $A_0 + \Delta A$ for the sub-layers penetrated by the inclusion and A_0 for the rest of the sub-layers.

Taking into account the Eqs. (A1), (A2) and the assumptions above, integrating the elastic energy (Eq.A1) over the monolayer thickness and minimizing it with respect to the area A and the curvature J of the bottom monolayer surface, we obtain the following expression for the spontaneous curvature.

$$J_s = \frac{\left\{(\lambda_0 L + \Lambda) \cdot \left[\frac{1}{2}\lambda_0 d \cdot (2L - d) + \Lambda z^*\right] - (\lambda_0 d + \Lambda)\left(\frac{1}{2}\lambda_0 L^2 + \Lambda z^*\right)\right\} \cdot \frac{\Delta A}{A_0}}{\left[(\lambda_0 L + \Lambda)\left(\frac{1}{3}\lambda_0 L^3 + \Lambda z^{*2}\right) - \left(\frac{1}{2}\lambda_0 L^2 + \Lambda z^*\right)^2\right] +}$$

$$\left[\left(\frac{1}{3}\lambda_0 L^3 + \Lambda z^{*2}\right)(\lambda_0 d + \Lambda) - \left(\frac{1}{2}\lambda_0 L^2 + \Lambda z^*\right)\left(\frac{1}{2}\lambda_0 d(2L - d) + \Lambda z^*\right)\right] \cdot \frac{\Delta A}{A_0} \quad \text{(A3)}$$

Our approach neglects the energy of transverse shear deformations of the monolayer matrix, which are also generated by the inclusion. This neglecting can be justified only for the case of small inclusions, such as the hydrophobic appendages of C2 domains (S8), whose in-plane dimensions do not exceed the characteristic decay length of membrane deformations. The latter can be estimated through the lipid monolayer elastic moduli of splay (bending), $\kappa \approx 4 \cdot 10^{-20}$ J (see e.g.(S7)), and tilt, κ_t (S9), as $\sqrt{\kappa / \kappa_t} \approx 1$nm (S9). In this case also the area of the membrane fragment deformed by the insertion will have an area of the order of square of the decay length, i.e. the fragment will constitute of just few lipid molecules. The more general model accounting for the spontaneous curvatures generated by larger inclusions will be published elsewhere.

Eq. (A3) allows us to estimate the spontaneous curvature J_s^{syt} generated by a C2AB domain. According to (S8) a double C2 domain binds 2 lipid polar heads meaning that $A_0 \approx 1.4$ nm^2. Estimations based on the structural data (S8) shows that after insertion of the hydrophobic appendages, the area of the complex between a double C2 domain and two lipid molecules becomes $A_0 + \Delta A = 2$ nm^2, meaning that $\Delta A \approx 0.6$ nm^2. Finally, the appendage penetrate about a third of the monolayer thickness meaning that $d = \frac{1}{3}L$ (S8). Assuming that $\frac{\Lambda}{\lambda_0 L} >> 1$ (the region around the plane of glycerol backbones is much more rigid than the rest of the monolayer matrix) and inserting the above values into the Eq.(A3) we obtain that the synaptotagmin spontaneous curvature is close to the inverse monolayer thickness, $J_s^{syt} \approx 1/L \approx 0.7$ nm^{-1}.

Estimation of the coverage of membrane surface by syt1 in tubes of 17nm diameter

Based on the determined above value of the synaptotagmin spontaneous curvature $J_s^{syt} \approx 0.7$ nm^{-1}, we can estimate the membrane area, which has to be covered by syt1 in order to stabilize the 17 nm tubules, which can be characterised by the radius and the curvature of the membrane mid surface equal to $R_t \approx 7$ nm and $J_t = 1/R_t \approx 0.14$ nm^{-1}, respectively. The curvature of a stress-free bilayer can be expressed through the spontaneous curvatures of its outer, J_s^{out}, and inner, J_s^{in}, monolayers by $J_t = (J_s^{out} - J_s^{in})/2$ (S10). The spontaneous curvature of the external monolayer containing syt1, J_s^{out}, can be presented as $J_s^{out} = J_s^0 + \phi \cdot J_s^{syt}$, where ϕ is the monolayer area fraction covered by syt1 and J_s^0 is the monolayer spontaneous curvature in the absence of synaptotagmin (S11). The spontaneous curvature of the

inner monolayer, which does not contain synaptotagmin, is $J_s^{in} = J_s^0$. Taken together the above relationships show that the curvature of the unstressed tubular membrane is $J_t = \phi \cdot J_s^{syt}/2$. Using the above values for J_s^{syt} and J_t, we obtain $\phi = 0.4$, meaning that about 40% of the tubular surface has to be covered by synaptotagmin.

Estimation of the effect of syt1 induced buckling on the energy barrier for hemifusion

We assume that the forming dimple is similar to the end-caps of the tubules generated by syt1 in our liposome tubulation experiments, and, therefore the curvature radius of its external surface is about 10 nm. Matching the stalk configuration (S*12*) to the buckled surface we find the membrane area, which undergoes unbending in the course of stalk formation, and estimate the released energy to be $20\,\mathrm{k_B T}$. This reduces the overall energy of stalk formation from, approximately, $40\,\mathrm{k_B T}$ (S*12*) to about $20\,\mathrm{k_B T}$.
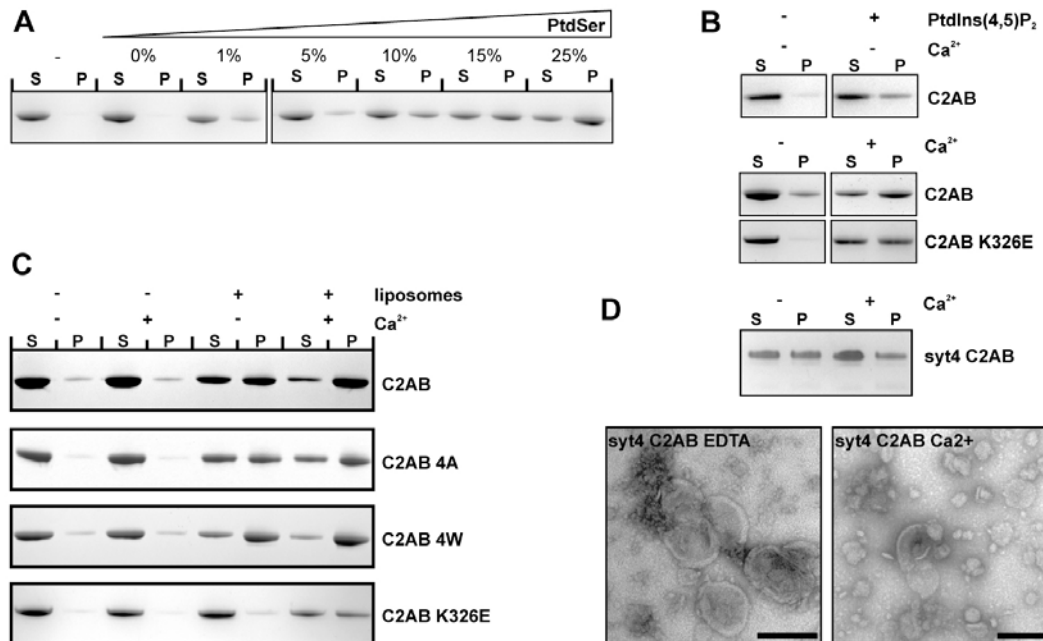
Fig. S1
Characterisation of liposome binding by wild type and mutant syt1.
(A) PtdSer (PS) dependence of lipid binding by syt1 in the presence of 1mM Ca^{2+} determined by liposome co-sedimentation assays. The numbers above the gels indicate the PtdSer content in the liposomes. These liposomes contained no $PtdIns(4,5)P_2$. (B) Ca^{2+}-independent binding to liposomes can be mediated by $PtdIns(4,5)P_2$ as determined by lipid co-sedimentation. Ca^{2+}-independent $PtdIns(4,5)P_2$ binding was abolished by the K326E mutation. The liposomes in the upper panel contained either no $PtdIns(4,5)P_2$ or 5% $PtdIns(4,5)P_2$ respectively. The liposomes in the lower panel contained 5% $PtdIns(4,5)P_2$ and 15% PtdSer. (C) Co-sedimentation assay using Folch liposomes and the indicated proteins. Ca^{2+} was added to a final concentration of 1mM. (D) Lipid co-sedimentation and electron micrographs showing liposome tubulation of Folch liposomes incubated with the syt4 C2AB domain. Ca^{2+} was added to a final concentration of 1mM. All liposomes shown in Fig. S1 were extruded through an 800nm filter.
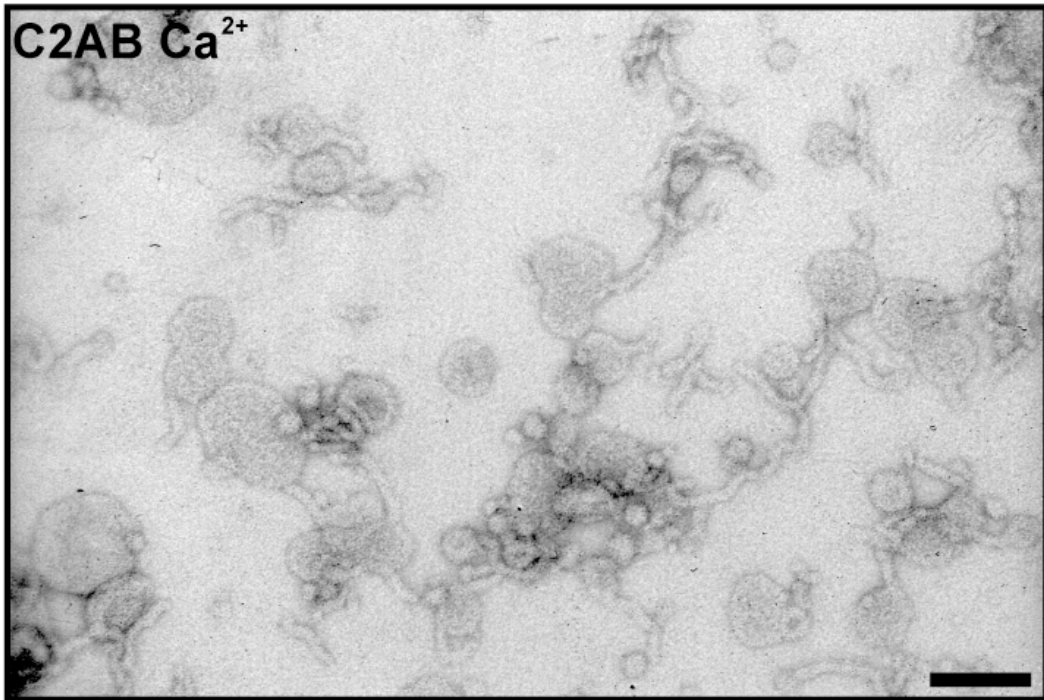
9
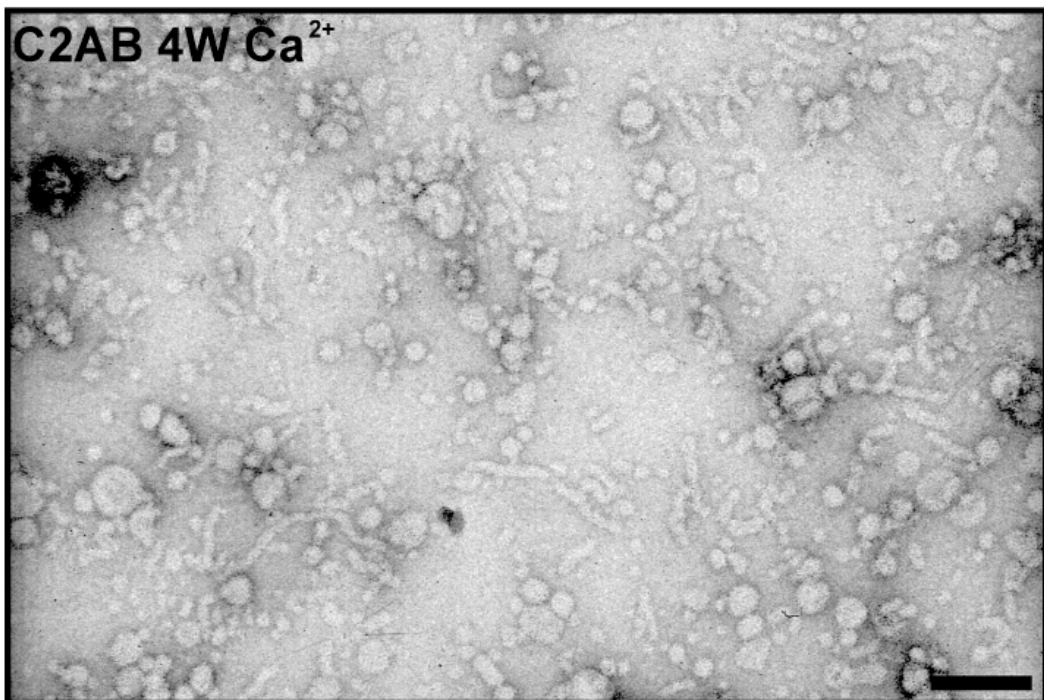
Fig. S2
Enhanced vesiculation of Folch liposomes by the 4W mutant.
Electron micrographs of Folch liposomes incubated with 10µM of the indicated proteins. Scale bar: 100nm.
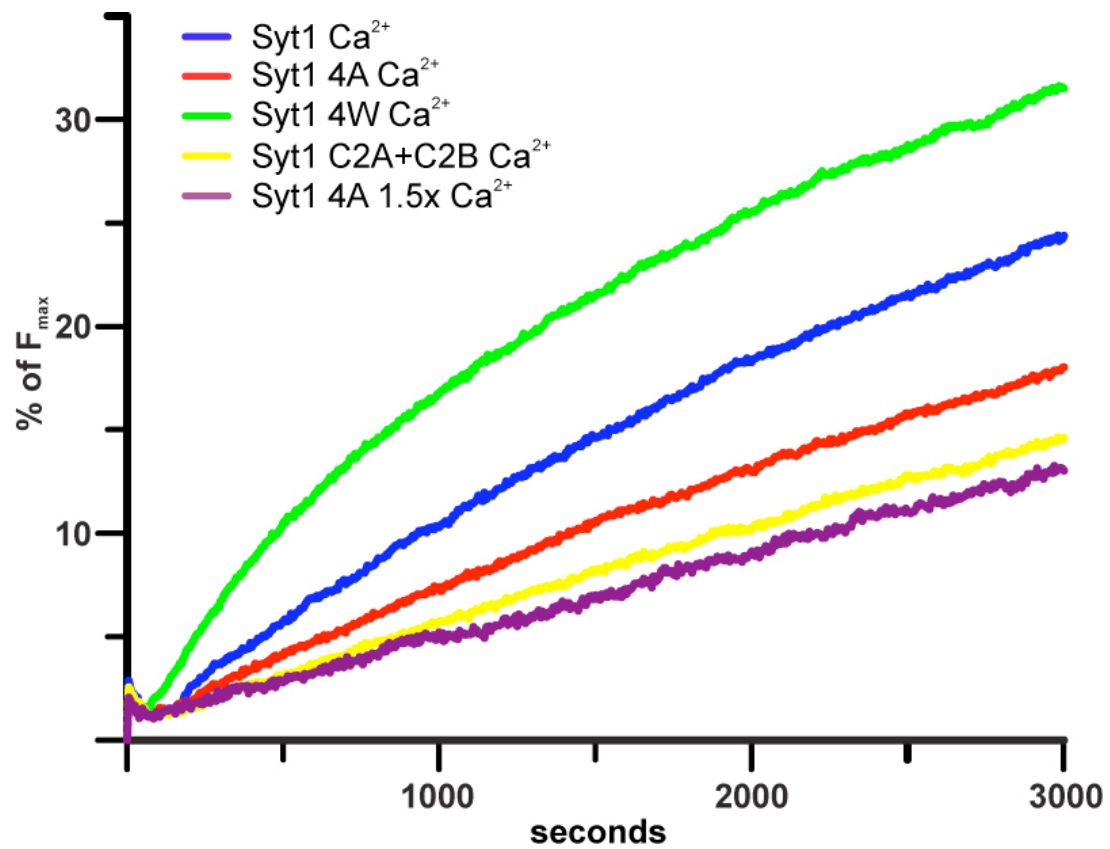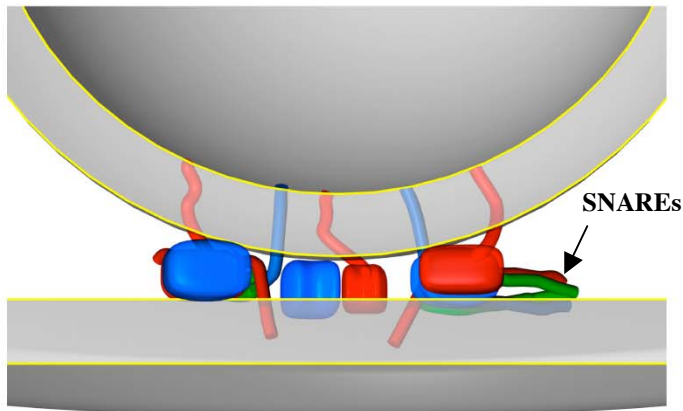
Fig. S3
Promotion of SNARE-mediated membrane fusion *in vitro* by wild type and mutant syt1.
In vitro membrane fusion assay as described in the Material and Methods using the indicated proteins at a concentration of 7.5μM. 1.5x syt4A was used at a concentration of 11.25μM. All experiments were conducted in the presence of 500μM Ca^{2+}.
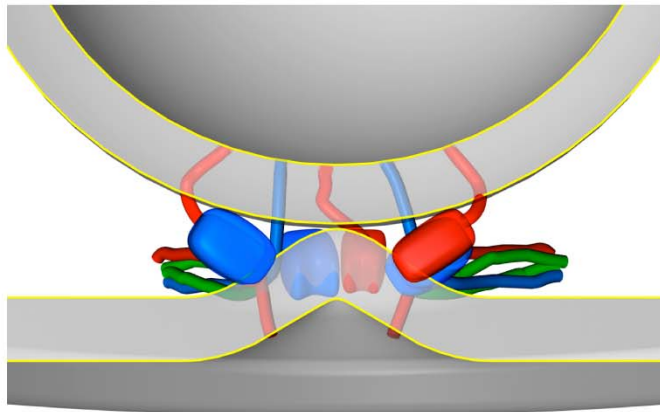
i) docked stage

Ca^{2+}

↓

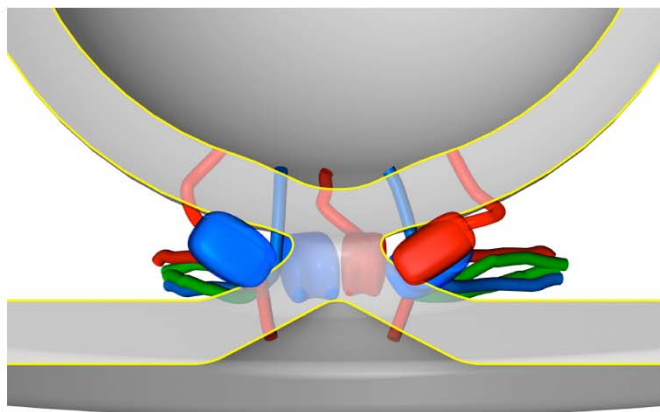# ii) Ca^{2+}-induced buckling

iii) hemifusion stage

Fig. S4
Model for the function of syt1 during Ca^{2+}-induced membrane fusion of synaptic vesicles.
(i) Prior to the Ca^{2+}-trigger, synaptic vesicles are docked and primed for release and the SNARE bundle is already partially assembled holding the two membranes about 3-4 nm apart. In this state syt1 (C2 domains shown as blue and red ovals, the syt1 transmembrane domain is shown in red and the intra-lumenal domain of syt1 is omitted) may interact in a Ca^{2+}-independent manner with the SNARE complex and possibly with plasma membrane PtdIns(4,5)P$_2$. (ii) Upon Ca^{2+} influx, syt1 changes its orientation and inserts the loops surrounding the Ca^{2+}-binding pockets into the plasma membrane. The insertion works like a wedge in the membrane leaflet and as a result the plasma membrane is buckled towards the vesicle which is held in place by the SNARE complex. (iii) This will induce curvature stress in the plasma membrane and a closer proximity of the two membranes thus leading to dramatically increased hemifusion fusion probability, leading to full fusion and thus exocytosis.
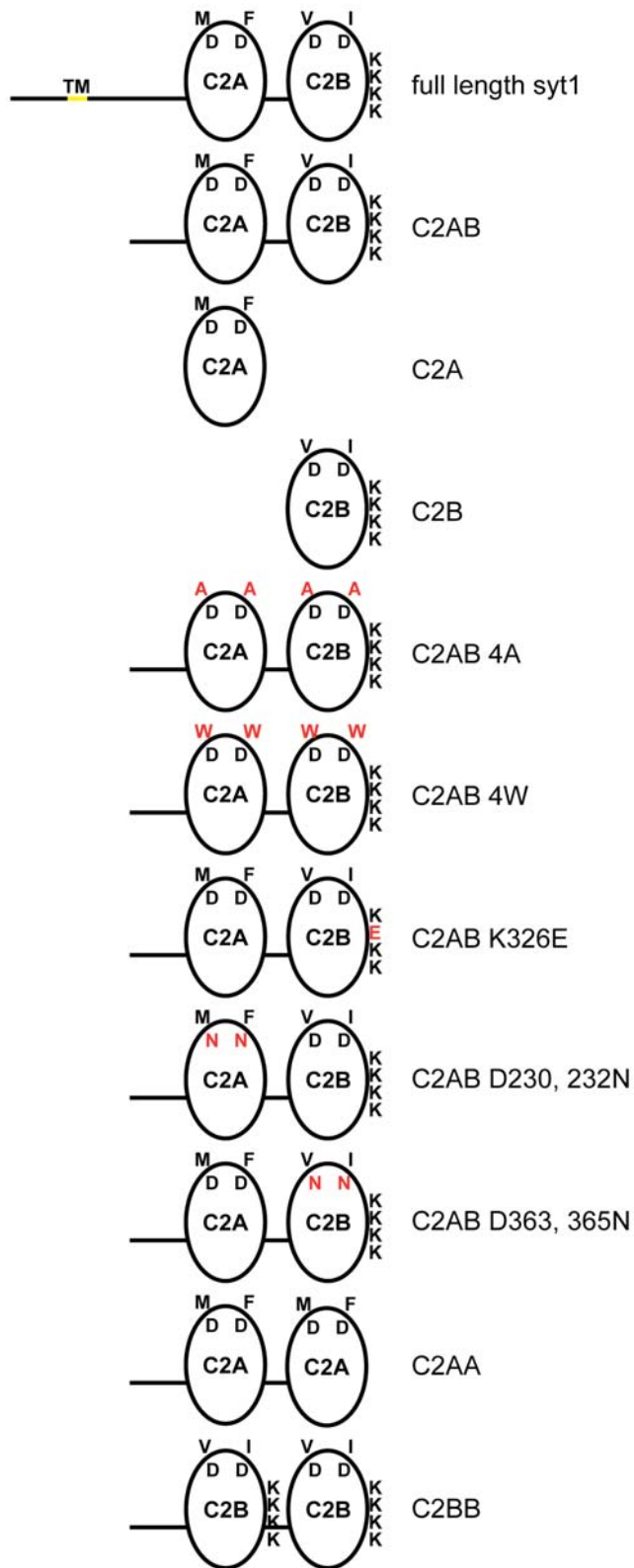
Fig. S5
A list of all syt1 fragments and mutants used in this study.
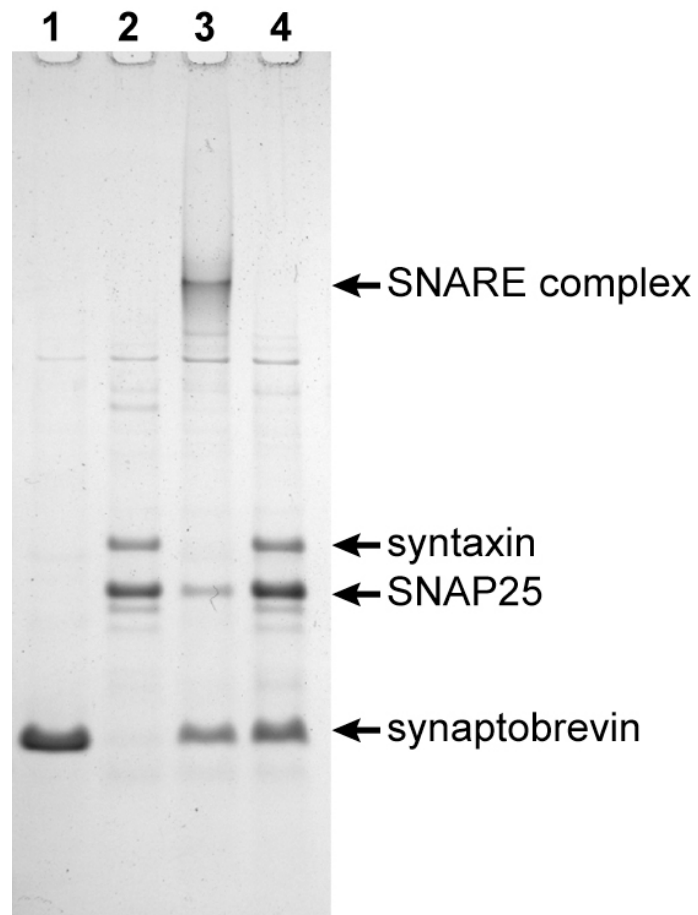For details of their construction refer to the Material and Methods.

Fig. S6
Coomassie stained SDS-PAGE gel showing the functionality of the full length SNARE molecules used in this study.
For detail of their construction and purification refer to the Material and Methods. 1. synaptobrevin. 2. tSNARE complex. 3. synaptobrevin + tSNARE complex incubated for 30 minutes at 37°C. 4. synaptobrevin + tSNARE complex incubated for 30 minutes at 37°C and subsequently boiled for 5 minutes.

References

S1.   C. Rickman, M. Craxton, S. Osborne, B. Davletov, *Biochem. J.* **378**, 681 (2004).

S2.   T. Hayashi *et al.*, *Embo J* **13**, 5051 (1994).

S3.   A. Bhalla, M. C. Chicka, W. C. Tucker, E. R. Chapman, *Nat. Struct. Mol. Biol.* **13**, 323 (2006).

S4.   D. Arac *et al.*, *Nat. Struct. Mol. Biol.* **13**, 209 (2006).

S5.   M. Spivak, *A Comprehensive introduction to differential feometry* (Brandeis University, 1970), pp.

S6.   M. M. Kozlov, M. Winterhalter, *J. Phys.II France* **1**, 1085 (1991).

S7.   S. Leikin, M. M. Kozlov, N. L. Fuller, R. P. Rand, *Biophys. J.* **71**, 2623 (1996).

S8.   D. Z. Herrick, S. Sterbling, K. A. Rasch, A. Hinderliter, D. S. Cafiso, *Biochemistry* **45**, 9668 (2006).

S9.   M. Hamm, M. Kozlov, *European Physical J. B* **6**, 519 (1998).

S10.   L. V. Chernomordik, M. M. Kozlov, *Annu. Rev. Biochem.* **72**, 175 (2003).

S11.   M. M. Kozlov, W. Helfrich, *Langmuir* **8**, 2792 (1992).

S12.   Y. Kozlovsky, M. M. Kozlov, *Biophys. J.* **82**, 882 (2002).